NEOPLASIA
www.neoplasia.com

Volume 17 Number 8 August 2015 pp. 625–633 625

Modeling Selective Elimination of Quiescent Cancer Cells from Bone Marrow

Stephen P. Cavnar[*,†], Andrew D. Rickelmann[‡,§], Kaille F. Meguiar[‡,§], Annie Xiao[‡,§], Joseph Dosch[‡], Brendan M. Leung[*,†], Sasha Cai Lesher-Perez[*,†], Shashank Chitta[‡,§], Kathryn E. Luker[‡,¶], Shuichi Takayama[*,†,¶] and Gary D. Luker[*,‡,§,#]

[*]Department of Biomedical Engineering, University of Michigan College of Engineering, Ann Arbor, MI 48109; [†]Biointerfaces Institute, University of Michigan College of Engineering, Ann Arbor, MI 48109; [‡]Department of Radiology, University of Michigan School of Medicine, Ann Arbor, MI 48109; [§]Center for Molecular Imaging, Department of Radiology, University of Michigan Medical School, Ann Arbor, MI 48109; [¶]Department of Macromolecular Science and Engineering, University of Michigan College of Engineering, Ann Arbor, MI 48109; [#]Department of Microbiology and Immunology, University of Michigan Medical School, Ann Arbor, MI 48109

Abstract

Patients with many types of malignancy commonly harbor quiescent disseminated tumor cells in bone marrow. These cells frequently resist chemotherapy and may persist for years before proliferating as recurrent metastases. To test for compounds that eliminate quiescent cancer cells, we established a new 384-well 3D spheroid model in which small numbers of cancer cells reversibly arrest in G1/G0 phase of the cell cycle when cultured with bone marrow stromal cells. Using dual-color bioluminescence imaging to selectively quantify viability of cancer and stromal cells in the same spheroid, we identified single compounds and combination treatments that preferentially eliminated quiescent breast cancer cells but not stromal cells. A treatment combination effective against malignant cells in spheroids also eliminated breast cancer cells from bone marrow in a mouse xenograft model. This research establishes a novel screening platform for therapies that selectively target quiescent tumor cells, facilitating identification of new drugs to prevent recurrent cancer.

Neoplasia (2015) 17, 625–633

Introduction

At time of diagnosis, up to 60% of breast cancer patients harbor disseminated tumor cells (DTC) in bone marrow in the absence of overt metastases [1].Histology typically shows DTC as single, non-proliferating cells [2]. DTC may remain in a growth-arrested, viable state for years or decades before resuming proliferation, producing late onset metastases after years of apparent disease-free survival [3]. Cancer cells in bone marrow also may circulate to other sites to produce additional metastases [4]. Presence of DTC in bone marrow correlates with up to three-fold higher risk of recurrent, clinically detectable breast cancer metastasis [1]. Occult cancer cells in bone marrow also confer poor prognosis for patients with other malignancies including melanoma, lung, and prostate, emphasizing that DTC represent a significant threat for disease progression across multiple cancers [5–7].

Address all correspondence to: Gary D. Luker, MD, University of Michigan, Center for Molecular Imaging, 109 Zina Pitcher Place, A526 BSRB, Ann Arbor, MI 48109-2200.
E-mail: gluker@med.umich.edu
Received 30 June 2015; Revised 31 July 2015; Accepted 10 August 2015

1476-5586
http://dx.doi.org/10.1016/j.neo.2015.08.001

Mesenchymal stromal cells (MSC) critically regulate biology and drug resistance of DTC in bone marrow. Breast cancer cells localize adjacent to MSC, potentially displacing hematopoietic stem cells from protective bone marrow niches formed by MSC [8,9]. MSC promote quiescence of DTC in bone marrow, contributing to resistance of cancer cells to chemotherapy drugs that predominantly target proliferating cells [8,10]. Ten to 15% of patients with breast cancer continue to have detectable malignant cells in bone marrow even after therapy with persistent DTC correlating with elevated risk of recurrent disease and death [11]. Cancer chemotherapy damages MSC, decreasing proliferative potential of these cells and secretion of molecules that support hematopoietic stem cells [12]. To reduce breast cancer recurrences while minimizing acute and chronic toxicities, there is an unmet need to discover therapies that selectively eliminate quiescent DTC with minimal damage to non-proliferating bone marrow stromal cells.

Identification of treatments that selectively eliminate cancer cells from bone marrow is limited by the lack of facile, high throughput models that recreate quiescence of cancer cells and quantify toxicity to malignant and stromal cells. Prior studies have tested for compounds that overcome stromal-mediated drug resistance in two-dimensional co-cultures of cancer and stromal cells or cancer cells with conditioned medium [13,14]. While simple to implement, two-dimensional assays minimize key aspects of DTC in bone marrow, including quiescence, intercellular contacts, hypoxia, and mass transport limitations of drugs [15–17]. Marlow et al developed a three-dimensional co-culture system in which bone marrow stromal cells supported quiescence of breast cancer cells, but the assay format precludes large-scale screening of compounds [18]. None of these studies quantified toxicity of compounds to stromal cells in the same culture to select against compounds generally toxic to all cells.

To enable testing for single or combination treatments that selectively eliminate quiescent cancer cells from bone marrow, we established a 384-well spheroid co-culture model in which bone marrow MSC support viable, quiescent breast cancer cells. We implemented a dual-color click beetle luciferase assay to selectively quantify relative numbers of viable cancer and stromal cells in the same spheroid. Using this imaging method, we identified combinations of compounds that preferentially eliminated quiescent breast cancer cells from spheroids with minimal toxicity to quiescent MSC. A therapy identified in our spheroid model effectively eliminated breast cancer cells from bone marrow in mice, linking this *in vitro* technology to efficacy *in vivo*.

Materials and Methods

Reagents

We purchased all cell culture supplies from Life Technologies (Carlsbad, CA) unless otherwise stated. We obtained drugs, compounds, and hormone supplements from the following sources: AG-490, PD0325901, CP724714, MK-2206 2HCl, MK-8669, GDC-0941, BazedoxifeneHCl, Trametinib (GSK112021), and Fulvestrant from SelleckChem (Houston, TX); AMD3100 from Tocris Bioscience (Bristol, UK); SB-431542 from Cayman Chemical (Ann Arbor, MI), 4-hydroxytamoxifen and β-estradiol from Sigma Aldrich (St. Louis, MO); and cisplatin (NDC-0703-5748-11), paclitaxel (NDC-55390-304-50), and doxorubicin (NDC-0069-3030-20) from the University of Michigan Hospital Pharmacy as clinical formulations. We prepared 10 mM stocks of estrogen in ethanol, while we used other compounds in formulations supplied or specified by manufacturers. D-Luciferin was from Promega (Madison, WI).

Cell Lines and Reporters

We maintained all cells in 10% FBS (HyClone, ThermoScientific, Waltham, MA) DMEM (#11995, Life Technologies) supplemented with penicillin, streptomycin, and glutamine (Life Technologies). We passaged cells every 2 to 4 days by trypsinizing and resuspending. We obtained immortalized human bone marrow mesenchymal stromal cell line HS-5 and breast cancer cell lines MDA-MB-231 and T47D from the American Type Culture Collection. We used PCR to amplify click beetle green CBG99 and CBRed from plasmids pCBR-Basic and pCBG99-Basic, respectively (Promega). PCR primers for CBG99 were XbaI CBG99 forward 5′-ATTATCTA GAACCGCCATGGTGAAGCGTGAGAAAAATGTC-3′ and XbaI CBG99 reverse 5′- ATTATCTAGACTAACCGCCGGCC TTCTCCAACAATTG-3′. Primers for CBRed were XbaI CBR forward 5′-ATTATCTAGAACCGCCATGGTAAAGCGTGA GAAAAATGTC-3′ and XbaI CBR reverse 5′- ATTATCTAGAT TACTAACCGCCGGCCTTCACCAAC-3′. We digested these PCR products with XbaIfor ligation to the XbaI site of lentiviral vector FUW (gift of D. Baltimore) [19]. Plasmids Fucci C mKO2-hCdt1(30/120)/pCSII-EF-MCS and Fucci D mAcGFP-hGeminin(1/110)/pCSII-EF-MCS were a gift of A. Miyawaki [20]. We generated stable reporter cell lines by lentiviral transduction as described [21].

Spheroid Co-Culture Model

We formed spheroids in 384-well low volume, non-adhesive, round bottom plates (#3676; Corning Inc., Corning, NY), which we sterilized with UV radiation. To form 200 to 300 μm diameter spheroids, we seeded 1% MDA-MB-231 or 5% T47D cells expressing CBGreen and fluorescence ubiquination-based cell cycle indicators (FUCCI) with HS5 cells expressing CBRed for a total of 3×10^3 cells per well in spheroid medium: phenol red free DMEM (#31053; Life Technologies) supplemented with 1% FBS (HyClone), 0.1 nM estrogen, penicillin/streptomycin/glutamine (Life Technologies), and pyruvate to match all but the serum content and phenol in standard growth medium. The difference in percentage of cancer cells is based on initial viability of cells after seeding spheroids and brightness of CBGreen expression to optimize dual-color measurements. For both spheroid maintenance and drug treatments, we replaced spheroid media in each plate every other day for the duration of an experiment by removing up to 20 μl from each well and replacing it with 20 μl fresh spheroid medium. For long-term culture, we filled the outside wells around the periphery of the plate with medium only to minimize evaporation within experimental wells. We replicated each experimental condition in four to seven wells and performed experiments at least twice. We distributed controls both on the interior and exterior of each plate to account for any effects of position on bioluminescence signal.

We highlight the simplicity and flexibility of using existing, relatively low-cost, low-binding 384 round bottom plates to form co-culture spheroids and induce cancer cell quiescence. Facile, long-term culture is necessary for following quiescent cells, as changes in growth or death are prolonged. While the plates we selected were developed for chemical assays, the low-binding surface and optimal geometry facilitate formation of a single, uniform spheroid per well.

Spheroids in this format form rapidly (<24 hours); are stable for at least 16 days; and are amenable to high throughput manipulation and/or analyses (bioluminescence, fluorescence, colorimetric, etc). Historically, multiple spheroids have been formed in lower-throughput, non-adherent 96-well plates. However, the larger volumes of these wells and movement of spheroids within a well has limited the ease of exchanging medium, spheroid collection, and imaging. With our system, spheroids are geometrically restricted to the bottom and center of the small wells, facilitating rapid, albeit incomplete media exchange.

To test effects of single compounds or combinations, we formed spheroids for two days in spheroid medium before beginning treatments with compounds at indicated concentrations. To establish baseline bioluminescence before treatment, we quantified bioluminescence in two to four columns of each plate before adding compounds to remaining wells. We exchanged medium with fresh compounds diluted in spheroid medium every other day. For treatment and recovery experiments, we imaged bioluminescence after eight days of treatment and then exchanged 20 µl of media three times, which removes >99% of luciferin and compounds from each well. For recovery we continued exchange with fresh medium every other day for a total of six days.

Click Beetle Red and Green Bioluminescence Imaging

We captured all bioluminescence images with an IVIS Lumina Series III (Perkin Elmer, Waltham, MA) and analyzed data with Living Image 4.3.1. We separated signals from click beetle red and green luciferase as discussed previously [22]. Briefly, we replaced 5 µl of each 384 well with a 1:4 dilution of 150 µg/ml luciferin, resulting in 1:20 final dilution of luciferin. After incubating at 37°C for 5 minutes, we captured a 3-to 5-minute exposure with medium binning and either 520 nm or 680 nm band pass filters. For imaging in 2D standard culture conditions we used 1:100 final dilution of luciferin.

Quiescence, Dissociation, and Colony Outgrowth from Spheroids

To test reversibility of cancer cell quiescence, we formed spheroids of MDA-MB-231 or T47D cells as described above. After 2 and 10 days in spheroid culture, we performed two-photon fluorescence microscopy to determine cell cycle status of cancer cells based on FUCCI reporters (orange, G1; green, S/G2/M). On the same days, we dissociated parallel spheroids for colony outgrowth in optimal 2D growth conditions. To dissociate spheroids, we collected spheroids from a 384-well plate; washed in excess PBS; aspirated PBS; trypsinized briefly; and plated dissociated cells in six-well plates containing full growth medium. After 1, 4, and 8 days in adherent culture, we imaged FUCCI status of colonies using epifluorescence and cell proliferation with bioluminescence. For bioluminescence in 2D cultures, we used 1:100 final dilution of 150 µg/ml luciferin. We note that faster outgrowth of cancer cells in 2D cultures required discounting the CBRed image due to substantial CBGreen signal. After bioluminescence imaging, we replaced medium to remove luciferin.

Cytotoxicity Assays in Two-Dimensional Culture

We seeded a total of 1×10^4 cells per well in 96-well plates, using 4% MDA-MB-231 CBGreen cells co-cultured with HS5 cells. One day after plating cells, we treated cells with increasing concentrations of doxorubicin, cisplatin, or paclitaxel as listed in figure legends, while control wells received vehicle only (n = 4-6 per condition). We quantified cytotoxicity based on bioluminescence.

Animal Models of Bone Marrow Metastasis and Drug Treatment

All animal procedures were approved by the University of Michigan Committee for the Use and Care of Animals. To model bone marrow metastases in mice, we delivered 1×10^5 MDA-MB-231 cells expressing CBGreen and FUCCI in 100 µl 0.9% NaCl solution via intracardiac injection into the left ventricle of 5- to 9-week-old female NSG mice [23]. Three days after injection, we randomly assigned mice to treatment with a single dose of doxorubicin (5 mg/kg i.p.), five daily doses of trametinib (1 mg/kg by oral gavage), combined treatment with each drug, or vehicle controls. We formulated trametinib for gavage as described [24]. We used only a single dose of doxorubicin because multiple doses of this drug are toxic to NSG mice. One week after completing the last dose of trametinib or vehicle, we euthanized mice; recovered lower extremity bone marrow; and plated dissociated bone marrow in standard cell culture medium to allow growth of viable MDA-MB-231 breast cancer cells by bioluminescence after one week [23]. For flow cytometry analysis of bone marrow, we used PBS to flush bone marrow from the femur and tibia as described [25]. We analyzed 5×10^5 events per bone marrow sample using a BD FACS Aria II (Becton Dickenson, Franklin Lakes, NJ).

Fluorescence Microscopy

We captured all microscopic images of spheroids with an upright Olympus FVE1000 MPE using a 25× NIR corrected objective (XLPLN25XWMP, NA=1.05, Olympus, Tokyo, Japan). To facilitate semi-high-throughput upright immersion microscopy, we transferred spheroids from 384-well plates to low aspect ratio wells as we described previously [26]. For images of hCDT-mKO and hGeminin-AcGFP (FUCCI) cells, we used 920 nm excitation and collected emitted light in green (495-540 nm) and red (575-630 nm) channels. To limit signal attenuation throughout 150 µm stacks (5 µm step size), we used the Olympus Bright-Z function to adjust laser transmission to the sample and detector gain to maximize signal per slice. We used the same acquisition parameters for all spheroids compared within a single experiment. For epifluorescence images, we used an Olympus IX70 microscope with a 10× objective, imaging red and green channels.

Data Processing, Plotting, and Statistics

We used Microsoft Excel (Seattle, WA) to process bioluminescence photon flux data before plotting data using GraphPad Prism (San Diego, CA). We used GraphPad Prism for statistics and estimation of EC_{50} values using four-parameter non-linear regression without weighting on log-transformed concentration data. We generated surface plots with the surf function in MATLAB. All graphs display mean values ± SEM unless stated otherwise. We normalized curves to photon flux measurements obtained 2 and 10 days post seeding for growth and cytotoxicity assays in spheroids, respectively. We propagated errors along each point for normalization. We calculated well-by-well selectivity of compounds by taking the log2 transform of CBRed flux (R) divided by CBGreen flux (G). The log2 transformation normalized the distribution and facilitates visualization of results. We then subtracted the log2 ratio of the untreated control, which adjusted for differences in baseline CBRed and CBGreen brightness. Negative selectivity corresponded to either

preferential growth of the CBGreen cancer cells or death of the CBRed HS5 cells.

To quantify the fraction of cells in S/G2/M cells using the FUCCI reporter, a person blinded to experimental conditions manually counted the number of orange or green cells using images with pseudo-colored overlay. For 2D cultures, we quantified a single slice for multiple view fields. For spheroids, we quantified a slice every 15 μm through a 150 μm volume. We calculated the ratio of cells in G1/0 by dividing the number of green (G) cells divided by total orange and green (R+G) for each image. We noted very few cells with both green and orange, and we discounted these cells from calculations. For statistical comparisons of 2D monoculture and 3D co-culture FUCCI ratios we applied the *t* test in GraphPad Prism.

Results

Co-Culture Spheroid Model of Breast Cancer Quiescence in Bone Marrow

We generated spheroids combining both breast cancer cells (1–5% of total cells) and HS5 bone marrow MSC (HS5) in non-adherent 384-well plates, modeling small numbers of DTC in bone marrow while still providing sufficient imaging signal from cancer cells. We used an established reporter system for the cell cycle (FUCCI) that marks cells in G1/G0 and S/G2/M with red and green fluorescent proteins, respectively [20]. Relative to proliferating cells in two-dimensional culture, both MDA-MB-231 and T47D breast cancer cells in spheroids arrested in G1/G0 phase of the cell cycle within 48 hours as measured by significantly lower fractions of cells in S/G2/M($P < .05$) (Figure 1, *A* and *B*).Bioluminescence from click beetle green luciferase expressed in cancer cells confirmed minimal proliferation over 10 days in spheroid culture with doubling times of 9.1 and 10.2 days for MDA-MB-231 and T47D cells, which are ≈9 and 3 times longer than two-dimensional culture, respectively. Fluorescence and bioluminescence imaging showed normal proliferation of cancer cells when returned to standard two-dimensional culture even in the presence of HS5 cells, showing viability and reversible quiescence of tumor cells in spheroids (Figure 1, *C* and *D*). HS5 cells were essential for viability of breast cancer cells in spheroids because the same number of cancer cells died rapidly when placed alone into suspension culture (data not shown). These data establish a straightforward method to rapidly generate large numbers of three-dimensional co-cultures with reversibly quiescent breast cancer cells and bone marrow MSC.

Dual-Color Click Beetle Luciferase Imaging of Breast Cancer and MSC

To independently monitor viability of cancer cells and MSC in the same spheroid, we implemented dual-color bioluminescence imaging

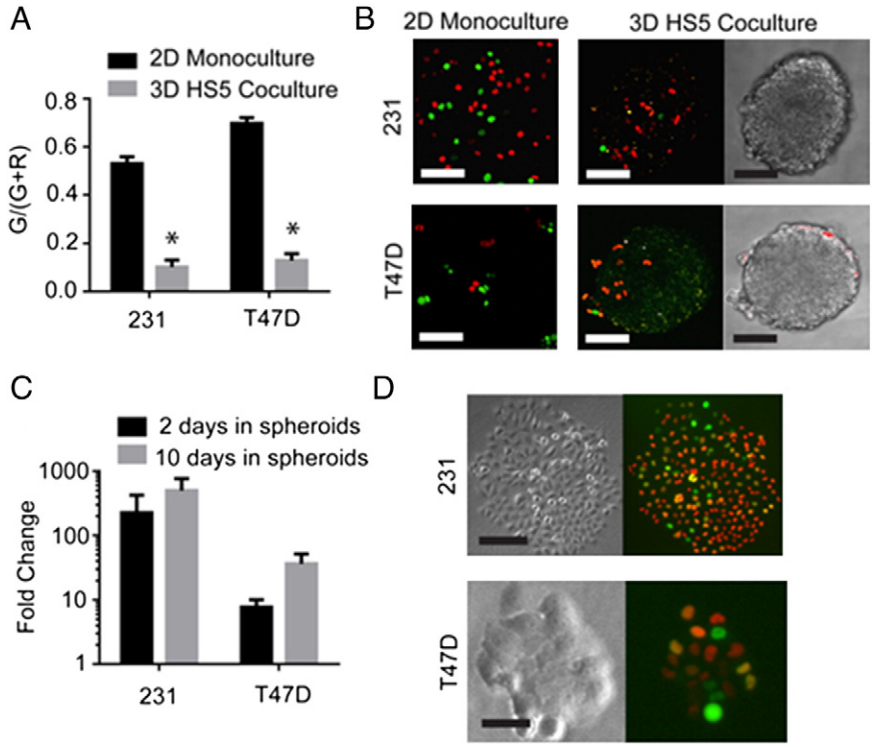

Figure 1. Bone marrow spheroids induce reversible quiescence of breast cancer cells. (A) Cell cycle status of MDA-MB-231 or T47D breast cancer cells in 2D culture or HS5 spheroids (3D z-stack) based on genetically-encoded FUCCI, which define cells in G1/G0 and S/G2/M phases based on red or green fluorescence, respectively. Graph shows mean values + SEM for fraction of cells in S/G2/M, which decreases for cancer cells in HS5 spheroids (n = 9-13 spheroids pooled from two independent setups; *t* test, * $P < .0001$ between 2D and 3D for both cell types). (B) Representative images of MDA-MB-231 and T47D FUCCI cells in 2D and 3D culture, respectively. Scale bars demarcate 100 μm. (C) MDA-MB-231 or T47D cancer cells were cultured in HS5 spheroids for 2 or 10 days, dissociated as a co-culture, then returned to adherent 2D growth conditions for 8 days. Data are plotted as mean values + SEM for fold change in bioluminescence over 8 days in adherent 2D co-culture (n = 6 measurements pooled from two independent setups, four spheroids dissociated per measurement). (D) Representative FUCCI images of outgrowth colonies from cancer cells described in panel C. Scale bars demarcate 200 μm and 50 μm for the MDA-MB-231 and T47D colonies, respectively.

with green (CBGreen) and red (CBRed) spectral variants of click beetle luciferase [27] (Figure 2). Similar to firefly luciferase, click beetle green and red luciferases are ATP-dependent enzymes that sensitively quantify relative numbers of viable cells. To characterize our ability to independently measure each enzyme without spectral deconvolution, we generated spheroids with increasing percentages of MDA-MB-231 or HS5 cells expressing CBGreen or CBRed, respectively. Signal increased linearly in both the 520 nm (green) and 680 nm (red) channels with increasing percentages of CBGreen cancer cells (Figure 2, *A* and *B*). Conversely, increasing the fraction of CBRed HS5 cells produced corresponding increases in red signal with negligible signal in the green channel (Figure 2*C*). CBGreen produces an order of magnitude less signal than CBRed when cancer cells are seeded at 1% to 10% of total cells in a spheroid (Figure 2*B*). These results establish that CBRed signal from HS5 cells does not affect detection of CBGreen from cancer cells, and CBGreen signal from cancer cells contributes substantially to the red channel only when spheroids contain greater than 10% cancer cells. By maintaining 1% to 5% cancer cells in spheroids, we can quantify linear changes in cancer cell bioluminescence without affecting signal detected from MSC.

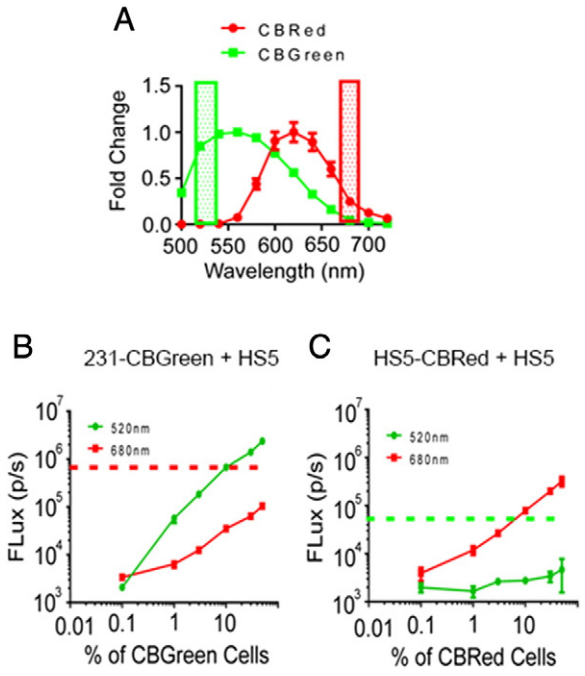

Figure 2. Validation of dual-color click beetle luciferase imaging for selective monitoring of cancer cells in bone marrow co-culture spheroids. (A) Representative bioluminescence spectra of MDA-MB-231 or HS5 cells expressing click beetle red or green luciferases, respectively. The spectra are normalized to their maxima for viewing purposes. The green and red boxes designate the band-pass filters used for separating cancer (CBGreen) and stromal (CBRed) components, respectively. Each data point represents mean ± SEM (n = 4 per point). (B) We plated an increasing percentage of MDA-MB-231 CBGreen cells with non-bioluminescent HS5 cells and quantified bioluminescence in green (520 nm) and red (680 nm) channels. Graphs in B and C show mean values with error bars smaller than the symbol when not evident (n = 20 per point). The red dashed line shows the typical photon flux from CBRed HS5 cells when these cells are present at proportions (95% to 99% of cells) used in our spheroids. (C) Increasing the percentage of HS5 CBRed cells with unmarked HS5 cells increases signal in the red channel only. The green dotted line shows the approximate average CBGreen photon flux when cancer cells are present at typical proportions (1% to 5% of cells). At ratios of cancer to stromal cells used in bone marrow spheroids, bioluminescence from stromal cells is undetectable in the green channel, and cancer cells produce very minimal signal in the red channel.

Limited Selectivity of Many Compounds Against Quiescent Cancer Cells

We initially tested standard chemotherapy drugs used in breast cancer for cytotoxicity against quiescent breast cancer cells in bone marrow spheroids, using bioluminescence from CBGreen and CBRed to quantify effects on cancer and HS5 cells, respectively. We plotted the untreated- and background-normalized dose-response curves for bioluminescence from both cancer and HS5 cells (Figure 3, *A*–*C*). To quantify selectivity of a drug for cancer cells at defined concentrations, we calculated the log-2-scale ratio of stromal to cancer bioluminescence. Log-2 normalization is typical for bioinformatics measures that compare to internal references [28].Selectivity is zero for untreated spheroids as both dose-response curves start at one. Bioluminescence <1% of starting values produces high variability as the signal is close to background of the imaging system, so we removed these selectivity points from graphs.

Cisplatin and paclitaxel produced higher EC_{50} values forquiescent MDA-MB-231 cells than HS5 cells in spheroids, resulting in negative selectivity and greater toxicity of these drugs to HS5 cells (Figure 3, *A*–*C*; EC_{50} values listed in Table S1). Doxorubicin had minimally positive selectivity for MDA-MB-231 cells in spheroids, potentially because this drug has multiple mechanisms of action unlike the predominantly cell-cycle dependent cytotoxicity of cisplatin and paclitaxel (Figure 3*B*). EC_{50} values for all drugs against cancer cells were notably higher in spheroids than two-dimensional co-cultures of proliferating breast cancer cells and HS5 cells, highlighting protective effects of quiescence against standard chemotherapy drugs (Table S1). We observed similar effects of these drugs on quiescent T47D cells in spheroids (Figure S1, *A*–*C*). We note that HS5 cells also remain quiescent in spheroids, so drug sensitivities are not caused by differences in proliferation between cancer and stromal cells.

We then tested molecularly-targeted compounds under development or clinically-approved for cancer therapy, including inhibitors of PI3-kinase, mTOR, TGF-β, Her2, and CXCR4 (Tables S2-5). Estrogen receptor (ER) inhibitors did not affect viability of quiescent ER^+ T47D cells in bone marrow spheroids, similar to persistence of ER^+ breast cancer cells in patients treated with these drugs. Several compounds non-selectively targeted both cancer cells and stromal cells or preferentially eliminated stromal cells (Figure S2, S3; Tables S3, S4). MEK inhibitor PD0325901 showed strong selectivity for quiescent MDA-MB-231 cells, likely because these cells constitutively activate this kinase downstream of mutant KRas (Figure 3*D*) [29]. Collectively, these results highlight the utility of our dual color imaging strategy to differentially measure effects of compounds on quiescent cancer versus stromal cells.

Combination Treatments Increase Selectivity In Vitro

To improve selective elimination of quiescent MDA-MB-231 cells, we incubated cells with increasing concentrations of PD0325901 and doxorubicin alone or in combination for 8 days. After removing compounds, we cultured spheroids for an additional 6 days to identify delayed effects on cell viability, similar to patients treated with

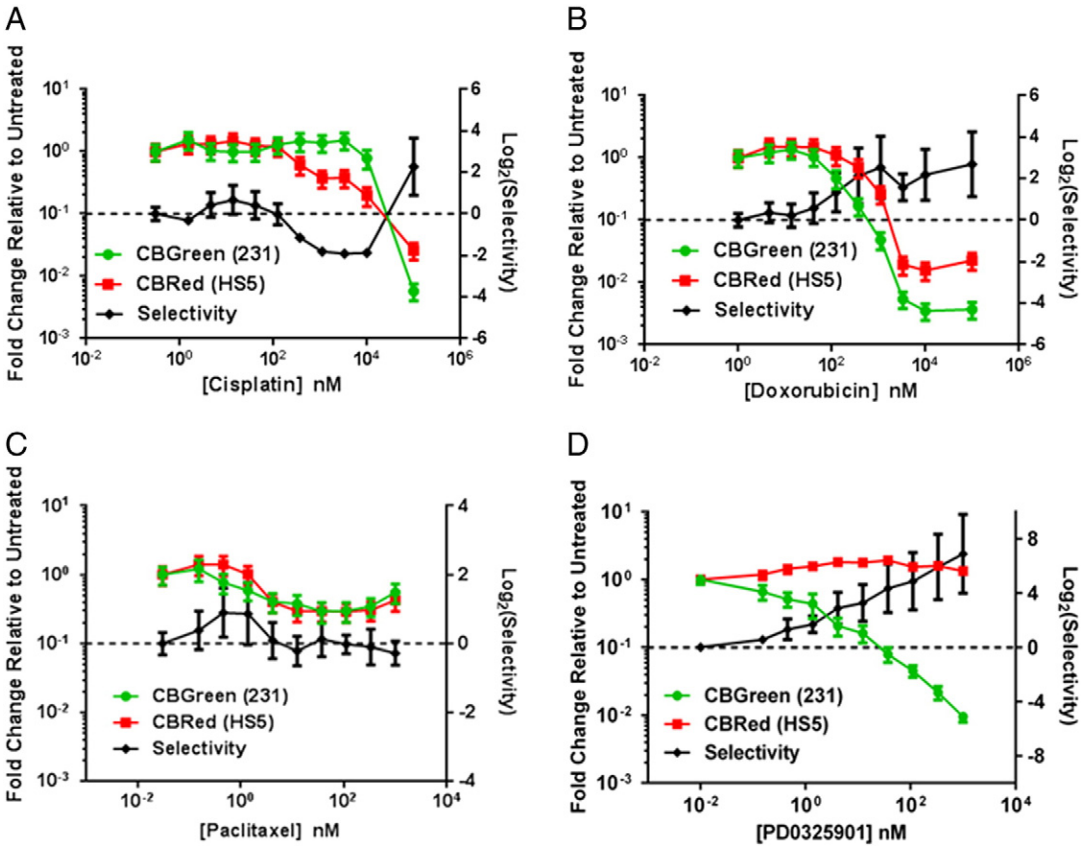

Figure 3. Responses of breast cancer and bone marrow stromal cells to single agent treatment in spheroids. (A-D) We treated spheroid co-cultures of 1% MDA-MB-231 cells and HS5 bone marrow stromal cells with listed concentrations of cisplatin (A), doxorubicin (B), paclitaxel (C), or PD0325901 (D) for eight days and then quantified CBGreen and CBRed bioluminescence, respectively (n = 7 spheroids per condition). Graphs display mean values + SEM for fold change in bioluminescence relative to vehicle control for each cell type. To directly demonstrate selective elimination of cancer cells, we plotted the $\log_2$ ratio of stromal to cancer bioluminescence (black line) with positive values showing preferential toxicity to cancer cells relative to HS5 stromal cells. Negative selectivity indicates that the counterpart CBRed stromal dose-response would be left-shifted relative to the depicted CBGreen curve. The dashed line shows no selectivity (equal effects of a compound on cancer and stromal cells).

intermittent cycles of chemotherapy. We observed maximum selectivity of ~4.0 for 100 nM PD0325901 alone after eight days of treatment (Figure 4*A*). Selectivity for intermediate concentrations of PD0325901 decreased after six days of recovery, potentially due to cytostatic rather than cytotoxic effects of this compound (Figure 4*B*). Conversely, selectivity elimination of MDA-MB-231 cells with

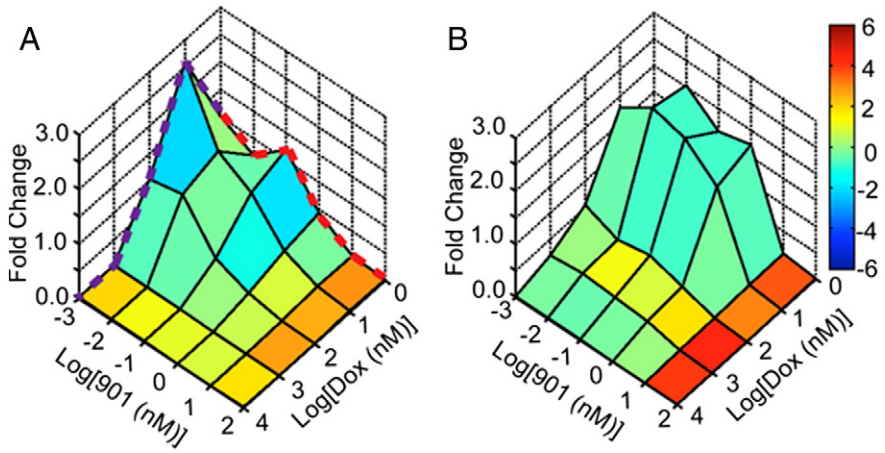

Figure 4. Enhanced selectivity of combinatorial treatments on cancer versus stromal cells in bone marrow spheroids after dosing and recovery. Surface plots show cancer cell bioluminescence (CBGreen) normalized to control after 8 days of treatment (A) and again after 6 days of recovery without compounds (B) for MDA-MB-231 cells treated with PD0325901 and doxorubicin. Selectivity is plotted on a pseudocolor scale with red and blue depicting highest and lowest selectivity of treatments for eliminating cancer versus stromal cells, respectively. The dotted purple and red lines in (A) represent the doxorubicin only and PD0325901 only curves, respectively.

doxorubicin alone increased after six days of recovery (Figure 4*B*). Combination treatment with 100 nM PD0325901 and 1 μM doxorubicin followed by six days of recovery produced peak selective toxicity to MDA-MB-231 cells (Figure 4B). Compensatory activation of MEK confers resistance to doxorubicin in several different cancers that we overcome by adding PD0325901 [30–32].

We also targeted Jak2 signaling in MDA-MB-231 cells since HS5 cells constitutively secrete IL6, a known activator of Jak2-Stat3 signaling in breast cancer progression [33–35]. While treatment with the Jak2 inhibitor AG490 produced minimal selectivity for cancer cells, we observed highest post-recovery selectivity for AG490 combined with doxorubicin (Figure S4). These results highlight how our system can identify combinations of compounds with greater toxicity to quiescent cancer versus stromal cells over extended periods of treatment and post-treatment recovery.

Bone Marrow Spheroid Model Predicts Combination Therapy Effective Against Bone Marrow Metastases

We tested combination therapy with MEK inhibition and doxorubicin on experimental bone marrow metastases with MDA-MB-231 cells. In a preliminary experiment with MDA-MB-231 cells expressing the FUCCI cell cycle reporter, flow cytometry of cancer cells recovered from lower extremity bone marrow of mice showed ~90% of MDA-MB-231 cells in G1/G0 of the cell cycle, similar to spheroids with HS5 cells. To replicate limited numbers of disseminated cancer cells in bone marrow, we injected MDA-MB-231 cells intracardiac into the left ventricle and began treatment three days later on mice assigned randomly to one of four groups: 1) single dose of doxorubicin; 2) five doses of trametinib (a clinically approved MEK inhibitor that closely replicates kinetics and functions of PD0325901); 3) single dose of doxorubicin and five doses of trametinib; or 4) vehicle only. After completing treatment and an additional week without treatment, we recovered and dissociated bone marrow from lower extremities and allowed outgrowth of cancer cells in standard two-dimensional cell culture. While we detected bioluminescent cancer cells from 7/10 cultures from vehicle control mice, treatment with doxorubicin or trametinib alone decreased numbers of positive mice to 3/8 and 5/11, respectively (Figure 5, *A–C*, and *E*). Notably, combination treatment with doxorubicin and trametinib completely eliminated outgrowth of MDA-MB-231 cells *in* vitro with bone marrow from 0/8 lower extremities positive for cancer cells (Figure 5, *D–E*) ($P < .05$).These results link efficacy of treatment combinations in our spheroid model to *in vivo* efficacy against cancer cells in bone marrow.

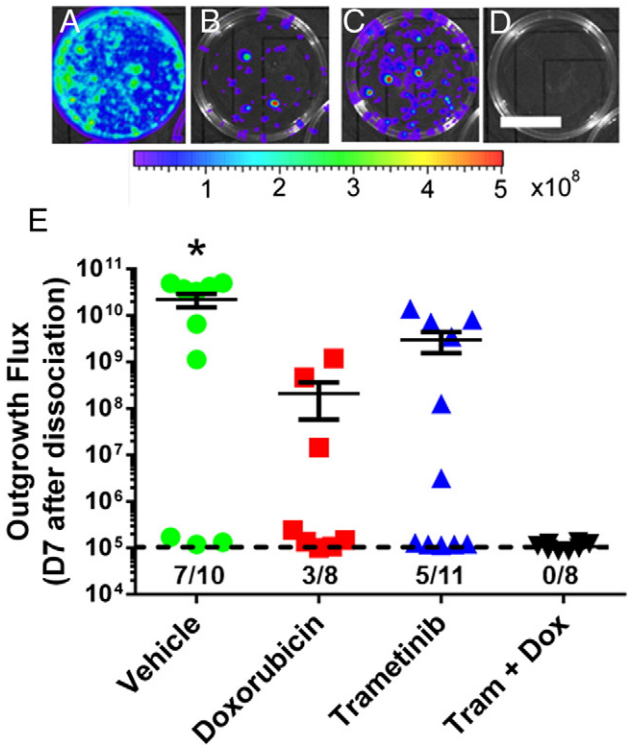

Figure 5. Combination treatment with doxorubicin and trametinib eliminates breast cancer cells from bone marrow. (A-D) We treated mice with experimental MDA-MB-231 bone marrow metastases with (A) vehicle control, (B), doxorubicin, (C) trametinib, or (D) both doxorubicin and trametinib. We recovered lower extremity bone marrow from mice and cultured cells ex vivo for seven days before quantifying bioluminescence from breast cancer cells. Plates show representative images from each treatment group. (E) Graph shows photon flux values for individual cultures from each treatment group. The fraction below each dataset represents the fraction of lower extremities from which we detected cancer cells above background (dotted line at 10^5). * denotes $P < .05$ by *t* test for difference between vehicle and other conditions.

Discussion

Selectively eliminating quiescent cancer cells from bone marrow and other potential sites of dormant tumor cells remains a major challenge in preventing recurrent cancer. Chemotherapeutic drugs for cancer typically interrupt functions of proliferating cells, such as mitosis, DNA replication, and mitogenic signaling that may be dispensable for survival of quiescent cancer cells. Drugs that effectively target quiescent cancer cells also may damage quiescent stromal cells essential for normal cellular environments, such as bone marrow MSC that establish protective niches for hematopoietic stem cells. Toxicity to normal tissues frequently limits drug dosage and/or frequency, impairing the ability to eliminate cancer cells. To successfully target dormant cancer cells in patients, there is a need for experimental models and techniques that establish quiescence of cancer cells and enable testing for compounds that kill malignant cells with minimal toxicity to stromal cells.

We meet this need with a novel combination of 3D co-culture spheroids and multi-modal imaging, establishing the first high throughput model for treatments that selectively eliminate quiescent cancer cells from bone marrow. Fluorescence imaging shows that ≈90% of MDA-MB-231 cells arrest in G1/G0 of the cell cycle in spheroids with bone marrow stromal cells, comparable to the cell cycle distribution of these cancer cells recovered from mouse bone marrow. While recognizing that co-culture spheroids of breast cancer and bone marrow stromal cells do not fully capture the cellular profile of bone marrow, this result shows our experimental system mimics the *in vivo* quiescent cell cycle profile of cancer cells in bone marrow. We optimized dual-color bioluminescence imaging parameters to independently quantify toxicity of compounds to breast cancer and bone marrow stromal cells in the same 384-well plate assay. The high sensitivity of bioluminescence imaging allowed us to readily measure very low numbers of cancer cells in spheroids (30–150 cancer cells per spheroid, or 1–5% of total cells). By forming spheroids with few cancer cells, we modeled rare numbers of quiescent cancer cells in bone marrow of patients. Measuring effects of treatments against both

cancer and normal bone marrow cells in the same spheroid eliminates the need for additional screening to avoid compounds that non-specifically kill all quiescent cells, saving time and resources. We expect this drug testing strategy will help investigators identify new compounds and drug combinations effective against dormant tumor cells with reduced toxicity to non- or slowly dividing cells in normal tissues.

To demonstrate applications of this bone marrow spheroid model for drug testing, we quantified effects of standard chemotherapeutic drugs used in breast cancer and representative molecularly-targeted agents under development or approved recently for patients. Although few tested compounds selectively eliminated cancer cells, we found combinations that improved elimination of MDA-MB-231 cells after sequential dosing and recovery. By measuring selectivity of responses in spheroids, we found that a MEK inhibitor plus doxorubicin enhanced elimination of breast cancer versus stromal cells and that an inhibitor of Jak2-Stat3 only selectively eliminated cancer cells in combination with doxorubicin. We tested the combination of MEK inhibitor and doxorubicin for effects against experimental bone marrow metastases in mice. Unlike single agent therapy, combined treatment with a MEK inhibitor and doxorubicin completely eliminated MDA-MB-231 cells from bone marrow. While additional validation is needed, this proof-of-concept experiment suggest that results from our new drug testing platform correlate with efficacy against cancer cells in mouse bone marrow.

We focused on modeling disseminated breast cancer cells in bone marrow because this is a recognized, clinically relevant site of tumor dormancy [3,36]. The model and imaging methods readily can be applied to other cancers with tumor dormancy, such as prostate and melanoma, and other anatomic sites that may harbor disseminated tumor cells [37,38]. Spheroids also can be generated with multiple types of stromal cells to reproduce more complex tumor environments and analyze toxicity of compounds to other types of stromal cells [15,39]. While established cell lines facilitate screening of multiple compounds to identify the best agents or combinations, patient-derived cancer cells could be integrated into co-culture spheroids for personalized drug testing, capitalizing on methods such as viral transduction to introduce imaging reporters [40]. Although click beetle bioluminescence only provides two-component resolution, this strategy may be multiplexed with other luciferase enzymes (e.g. NanoLuc or *Gaussia* luciferase) and/or fluorescence readouts to measure additional cell populations or specific drug targets [41–43].

Our high throughput, simple, long-term, 3D model of cancer cell quiescence is a significant advance over previous 2D systems and existing, more complex 3D models. The system facilitates maintenance of 384 well format cultures for at least 16 days, which enables extended dosing and recovery protocols to identify optimal drugs and drug combinations that selectively eliminate quiescent cancer cells. These 3D culture and imaging strategies are amenable to high throughput screening and co-culture models of other cancers and sites of tumor dormancy. Incorporating screening against quiescent cancer cells in a bone marrow environment early in drug development will increase the likelihood of finding therapies independent of cell division and with lower toxicity to normal tissues. We expect our drug testing platform will help advance more effective, less toxic therapies to clinical trials and ultimately clinical oncology.

Author Contributions

SPC, KEL, ST, and GDL conceived the project. SPC, KFM, and KEL developed and implemented the combined approach to dual-color bioluminescence imaging, fluorescence reporter imaging, and spheroid culture. SPC, KFM, ADR, AX, SC, and KEL conducted experiments, performed drug screening, analyzed data, and prepared figures. JD and KEL provided new reagents. SPC, ST, and GDL wrote the manuscript. All authors reviewed results, discussed impact, and commented on the manuscript.

Competing Financial Interests

The authors declare no competing financial interests.

Acknowledgments

This work was supported by United States National Institutes of Health grants R01CA170198 and 1S10RR028819. SPC was supported by a NSF predoctoral fellowship F031543 and the Advanced Proteome Informatics of Cancer Training Grant # T32 CA140044. We thank Judith Leopold for her helpful discussion of this work. We thank Aaron Robida and the University of Michigan Flow Cytometry Core for help optimizing analysis of bone marrow samples.

Appendix A. Supplementary Data

Supplementary data to this article can be found online at http://dx.doi.org/10.1016/j.neo.2015.08.001.

References

[1] Braun S, Vogl FD, Naume B, Janni W, Osborne MP, Coombes RC, Schlimok G, Diel IJ, Gerber B, and Begauer G, et al (2005). A pooled analysis of bone marrow micrometastasis in breast cancer. *N Engl J Med* **353**, 793–802.

[2] Pantel K and Alix-Panabieres C (2014). Bone marrow as a reservoir for disseminated tumor cells: a special source for liquid biopsy in cancer patients. *Bonekey Rep* **3**, 584.

[3] Zhang X, Giuliano M, Trivedi M, Schiff R, and Osborne C (2013). Metastasis dormancy in estrogen receptor-positive breast cancer. *Clin Cancer Res* **19**, 6389–6397.

[4] Pantel K, Alix-Panabieres C, and Riethdorf S (2009). Cancer micrometastases. *Nat Rev Clin Oncol* **6**, 339–351.

[5] Eide N, Faye R, Hoifodt H, Overgaard R, Jebsen P, Kvalheim G, and Fodstand O (2009). Immunomagnetic detection of micrometastatic cells in bone marrow in uveal melanoma patients. *Acta Ophthalmol* **87**, 830–836.

[6] Passlick B, Kubuschok B, Izbicki J, Thetter O, and Pantel K (1999). Isolated tumor cells in bone marrow predict reduced survival in node-negative non-small cell lung cancer. *Ann Thorac Surg* **68**, 2053–2058.

[7] Lilleby W, Stensvold A, Mills I, and Nesland J (2013). Disseminated tumor cells and their prognostic significance in nonmetastatic prostate cancer patients. *Int J Cancer* **133**, 149–155.

[8] Ono M, Kosaka N, Tominaga N, Yoshioka Y, Takeshita F, Takahashi H, Yoshida M, Tsuda H, Tamura K, and Ochiya T (2014). Exosomes from bone marrow mesenchymal stem cells contain a microRNA that promotes dormancy in metastatic breast cancer cells. *Sci Signal* **7**, ra63.

[9] Frenette P, Pinho S, Lucas D, and Scheiermann C (2013). Mesenchymal stem cell: keystone of the hematopoietic stem cell niche and a stepping-stone for regenerative medicine. *Annu Rev Immunol* **31**, 285–316.

[10] Braun S, Kentenich C, Janni W, Hepp F, de Wall J, Willgeroth F, Sommer H, and Pantel K (2000). Lack of effect of adjuvant chemotherapy on the elimination of single dormant tumor cells in bone marrow of high-risk breast cancer patients. *J Clin Oncol* **18**, 80–86.

[11] Mathiesen R, Borgen E, Renolen A, Lokkevik E, Nesland JM, Anker G, Ostenstad B, Lundgren S, Risberg T, and Mialland I, et al (2012). Persistence of disseminated tumor cells after neoadjuvant treatment for locally advanced breast cancer predicts poor survival. *Breast Cancer Res* **14**, R117.

[12] Cao J, Tao M, Yang P, Li W, Xia J, Du H, Tang W, Wang H, Chen W, and Xiao H (2008). Effects of adjuvant chemotherapy on bone marrow mesenchymal stem cells of colorectal cancer patients. *Cancer Lett* **263**, 197–203.

[13] McMillin D, Delmore J, Weisberg E, Negri JM, Geer DC, Klippel S, Mitsiades N, Schlossman RL, and Kung AL, et al (2010). Tumor cell-specific bioluminescence platform to identify stroma-induced changes to anticancer drug activity. *Nat Med* **16**, 483–489.

[14] Weisberg E, Liu Q, Zhang X, Nelson E, Sattler M, Liu F, Nicolais M, Zhang J, Mitsiades C, and Smith RW, et al (2013). Selective Akt inhibitors synergize with tyrosine kinase inhibitors and effectively override stroma-associated cytoprotection of mutant FLT3-positive AML cells. *PLoS One* **8**, e56473.

[15] Mehta G, Hsiao A, Ingram M, Luker G, and Takayama S (2012). Opportunities and challenges for use of tumor spheroids as models to test drug delivery and efficacy. *J Control Release* **164**, 192–204.

[16] Spencer J, Ferraro F, Roussakis E, Klein A, Wu J, Runnels JM, Zaher W, Mortensen LJ, Alt C, and Turcotte R, et al (2014). Direct measurement of local oxygen concentration in the bone marrow of live animals. *Nature* **508**, 269–273.

[17] Weiswald L, Bellet D, and Dangles-Marie V (2015). Spherical cancer models in tumor biology. *Neoplasia* **17**, 1–15.

[18] Marlow R, Honeth G, Lombardi S, Cariati M, Hessey S, Pipli A, Mariotti V, Buchupalli B, Foster K, and Buchupalli B, et al (2013). A novel model of dormancy for bone metastatic breast cancer cells. *Cancer Res* **73**, 6886–6899.

[19] Lois C, Hong E, Pease S, Brown E, and Baltimore D (2002). Germline transmission and tissue-specific expression of transgenes delivered by lentiviral vectors. *Science* **295**, 868–872.

[20] Sakaue-Sawano A, Kuorkawa H, Morimura T, Hanyu A, Hama H, Osawa H, Kashiwagi S, Fukami K, Miyata T, and Miyoshi H, et al (2008). Visualizing Spatiotemporal Dynamics of Multicellular Cell-Cycle Progression. *Cell* **132**, 487–498.

[21] Smith M, Luker K, Garbow J, Prior J, Jackson E, Piwnica-Worms D, and Luker G (2004). CXCR4 regulates growth of both primary and metastatic breast cancer. *Cancer Res* **64**, 8604–8612.

[22] Coggins NL, Trakimas D, Chang SL, Ehrlich A, Ray P, Luker KE, Linderman JJ, and Luker GD (2014). CXCR7 Controls Competition for Recruitment of β-Arrestin 2 in Cells Expressing Both CXCR4 and CXCR7. *PLoS One* **9**, e98328.

[23] Fenner J, Stacer A, Winterroth F, Johnson T, Luker K, and Luker G (2014). Macroscopic stiffness of breast tumors predicts metastasis. *Sci Rep* **4**, 5512.

[24] Kwong L, Costello JC, Liu H, Jiang S, Helms TL, Langsdorf AE, Jakubosky D, Genovese G, Muller FL, and Jeong JH, et al (2012). Oncogenic NRAS signaling differentially regulates survival and proliferation in melanoma. *Nat Med* **18**, 1503–1510.

[25] Ray P, Stacer AC, Fenner J, Cavnar SP, Meguiar K, Brown M, Luker KE, and Luker GD (2014). CXCL12-gamma in primary tumors drives breast cancer metastasis. *Oncogene* **34**, 2043–2051.

[26] Cavnar SP, Salomonsson E, Luker KE, Luker GD, and Takayama S (2014). Transfer, Imaging, and Analysis Plate for Facile Handling of 384 Hanging Drop 3D Tissue Spheroids. *J Lab Autom* **19**, 208–214.

[27] Miloud T, Henrich C, and Hammerling G (2007). Quantitative comparison of click beetle and firefly luciferases for in vivo bioluminescence imaging. *J Biomed Opt* **12**, 054018.

[28] Quackenbush J (2002). Microarray data normalization and transformation. *Nat Genet* **32**, 496–501.

[29] Scholl C, Frohling S, Dunn IF, Schinzel AC, Barbie DA, Kim SY, Silver SJ, Tamayo P, Wadlow RC, and Ramaswamy S, et al (2009). Synthetic Lethal Interaction between Oncogenic KRAS Dependency and STK33 Suppression in Human Cancer Cells. *Cell* **137**, 821–834.

[30] Choi J, Yip-Schneider M, Albertin F, Wiesenauer C, Wang Y, and Schmidt CM (2008). The effect of doxorubicin on MEK-ERK signaling predicts its efficacy in HCC. *J Surg Res* **150**, 219–226. http://dx.doi.org/10.1016/j.jss.2008.1001.1029 [Epub 2008 Mar 1013].

[31] McCubrey JA, Steelman LS, Chappell WH, Abrams SL, Wong EW, Chang F, Lehmann B, Terrian DM, Milella M, and Tafuri A, et al (2007). Roles of the Raf/MEK/ERK pathway in cell growth, malignant transformation and drug resistance. *Biochim Biophys Acta* **1773**, 1263–1284.

[32] Jin W, Wu L, Liang K, Liu B, Lu Y, and Fan Z (2003). Roles of the PI-3K and MEK pathways in Ras-mediated chemoresistance in breast cancer cells. *Br J Cancer* **89**, 185–191.

[33] Delk N and Farach-Carson M (2012). Interleukin-6: a bone marrow stromal cell paracrine signal that induces neuroendocrine differentiation and modulates autophagy in bone metastatic PCa cells. *Autophagy* **8**, 650–653.

[34] Roecklein BA and Torok-Storb B (1995). Functionally distinct human marrow stromal cell lines immortalized by transduction with the human papilloma virus E6/E7 genes. *Blood* **85**, 997–1005.

[35] Chang Q, Bournazou E, Sansone P, Berishaj M, Gao SP, Daly L, Wels J, Theilen T, Granitto S, and Zhang X (2013). The IL-6/JAK/Stat3 feed-forward loop drives tumorigenesis and metastasis. *Neoplasia* **15**, 848–862.

[36] Jung Y, Shiozawa Y, Wang J, McGregor N, Dai J, Park SI, Berry JE, Havens AM, Joseph J, and Kim JK, et al (2012). Prevalence of prostate cancer metastases after intravenous inoculation provides clues into the molecular basis of dormancy in the bone marrow microenvironment. *Neoplasia* **14**, 429–439.

[37] Ruppender N, Morrissey C, Lange P, and Vessella R (2013). Dormancy in solid tumors: implications for prostate cancer. *Cancer Metastasis Rev* **32**, 501–509.

[38] Ossowski L and Aguirre-Ghiso J (2009). Dormancy of metastatic melanoma. *Pigment Cell Melanoma Res* **23**, 41–56.

[39] Hirschhaeuser F, Menne H, Dittfeld C, West J, Mueller-Klieser W, and Kunz-Schughart L (2010). Multicellular tumor spheroids: an underestimated tool is catching up again. *J Biotechnol* **148**, 3–15.

[40] Nguyen L, Cox CL, Eirew P, Knapp D, Pellacani D, Kannan N, Carles A, Moksa M, Balani S, and Shah S, et al (2014). DNA barcoding reveals diverse growth kinetics of human breast tumour subclones in serially passaged xenografts. *Nat Commun* **5**.

[41] Luker K, Mihalko L, Schmidt B, Lewin S, Ray P, Shcherbo D, Chudakov D, and Luker G (2012). *Nat Med* **18**, 172–177.

[42] Hall M, Unch J, Binkowski BF, Valley MP, Butler BL, Wood MG, Otto P, Zimmerman K, Vidugiris G, and Machleidt T, et al (2012). Engineered luciferase reporter from a deep sea shrimp utilizing a novel imidazopyrazinone substrate. *ACS Chem Biol* **7**, 1848–1857.

[43] Ray P, Lewin S, Mihalko L, Schmidt B, Luker K, and Luker G (2011). Noninvasive imaging reveals inhibition of ovarian cancer by targeting CXCL12-CXCR4. *Neoplasia* **13**, 1152–1161.